THE JOURNAL OF PHYSICAL CHEMISTRY C

Article

pubs.acs.org/JPCC

Water Confined in Mesoporous TiO_2 Aerosols: Insights from NMR Experiments and Molecular Dynamics Simulations

Manuel I. Velasco,[†] M. Belén Franzoni,[†] Esteban A. Franceschini,[‡] Estefanía Gonzalez Solveyra,[§,∥] Damián Scherlis,[§,⊥] Rodolfo H. Acosta,*[,†] and Galo J. A. A. Soler-Illia*[,§,#]

[†]FAMAF, Universidad Nacional de Córdoba and IFEG-CONICET, 5016 Córdoba, Argentina

[‡]INFIQC-CONICET, Departamento de Fisicoquímica, Facultad de Ciencias Químicas, Universidad Nacional de Córdoba, Ciudad Universitaria, 5000 Córdoba, Argentina

[§]DQIAQF, Facultad de Ciencias Exactas y Naturales and [⊥]INQUIMAE, Facultad de Ciencias Exactas y Naturales, Universidad de Buenos Aires, Ciudad Universitaria, Pab. II, C1428EHA Ciudad Autónoma de Buenos Aires, Argentina

[∥]Department of Biomedical Engineering, Department of Chemistry and Chemistry of Life Processes Institute, Northwestern University, Evanston, Illinois 60209, United States

[#]Instituto de Nanosistemas, Universidad Nacional de General San Martín, Avenida 25 de Mayo y Francia, 1650 San Martín, Argentina

Supporting Information

ABSTRACT: The adsorption of water vapor in mesoporous TiO_2 was studied by nuclear magnetic resonance (NMR) and multiscale molecular dynamics simulations. Three different water environments were distinguished and quantified: a first layer, where strongly bound water molecules exist at the inner surfaces; a second less structured layer but still with restricted mobility; and a bulk-like fraction of mobile water. The obtained NMR results can be explained in the framework of molecular dynamics simulations that give insight on the filling mechanisms in TiO_2 nanoporous materials. For these highly hydrophilic materials, it is shown that adsorption isotherms may render a smaller effective pore size due to the presence of a layer of highly bound water. The synergistic combination of experimental NMR data and MD simulations renders a detailed analysis of the water dynamics inside the titania pore space.

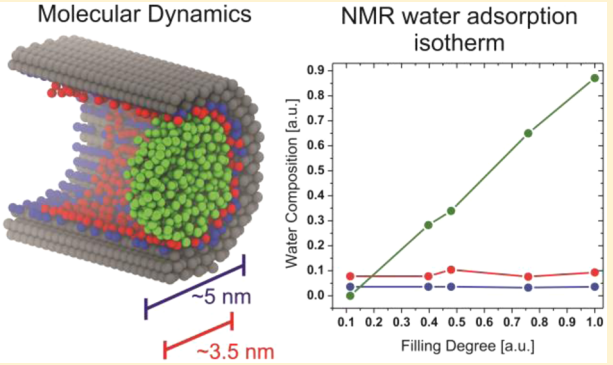

INTRODUCTION

Porous materials are of great interest because of their ability to interact with a variety of entities like atoms, ions, molecules, and nanoparticles, not only at the surfaces level but also in the bulk of the materials. Due to their tunable surface area, porosity, pore volume, pore shape, and framework compositions, mesoporous materials are currently under intense research. Some of the main areas where these materials are applied include catalysis, adsorption, or drug delivery.[1−7]

It is well known that mesopore size affects the thermodynamics, structural properties, and dynamics of liquids confined within them. In restricted geometries, water molecules interact with surfaces through hydrophobic, hydrophilic, or hydrogen bonds, where a competition between surface−liquid and liquid−liquid interactions is present. This leads to molecular structuring not observed in bulk water, which gives rise to partial ordering of water molecules in the vicinity of the confining surface.[8,9] In silica pores of 4.5 nm three different types of water were identified by measuring molecular correlation times by means of NMR relaxometry: an adsorbed layer, a second more mobile layer, and a third group of essentially free water.[10] Additionally, the filling of silica pores of 3.3 and 8 nm was also investigated by NMR spectroscopy, where two filling mechanisms were proposed. In narrow pores capillary condensation was preceded by monolayer coverage, whereas in the wider pores a radial thickening involving several layers was observed to take place before capillary condensation[11] Much insight on the filling mechanisms, structure, and dynamics of water in nanopores has been contributed by molecular dynamics and grand canonical Monte Carlo simulations.[12−21] The vast majority of this work has addressed silica pores with diameters in the range 1−4 nm.[12,13,16−21] These studies have found that in SiO_2 pores water organizes in two or three molecular layers at the interface with reduced mobility, of which the first one is considerably slower. Moreover, bulk-like behavior is already recovered in the core region in pores as small as 2 nm.[12,16−18] Molecular simulations

Received: January 23, 2017
Revised: March 9, 2017
Published: March 10, 2017

DOI: 10.1021/acs.jpcc.6b12511
J. Phys. Chem. C XXXX, XXX, XXX−XXX

of water in titania pores, on the other hand, have been much scarcer.[14]

Among the wide variety of materials, mesoporous TiO_2 is of particular interest due to its outstanding features such as low cost, environmental benignity, plentiful polymorphs, excellent chemical and thermal stability, biocompatibility, and tunable electronic and optical properties.[4,22,23] In consequence, TiO_2 mesoporous systems are of paramount importance in biomaterials, photocatalysis, solar cells, or solar fuel production.[24−26] However, due to the difficulty in obtaining mesoporous titanium dioxide with controlled mesopore size, titania systems have been less explored than their silica counterparts. The interaction of water with TiO_2 surfaces is three times stronger than with silica; thus, it is expected that the structured water layers will present an even lower mobility. Empirical observation of the water layer formation has been reported on photocatalityc films[27,28] and in the surface of TiO_2 nanoparticles.[29] Structuring of water in titania nanopores was first observed in molecular dynamic simulations, which have set a prediction of the structure, dynamics, and filling mechanism of water inside the nanopores.[14] There properties such as translational and rotational mobility and the liquid−vapor equilibrium of H_2O in fully and partially filled TiO_2 cylindrical pores of different sizes, ranging from 1.3 to 5.1 nm, were determined. It was also found that water forms three distinct layers: a first monolayer strongly immobilized on the interface, which reduces the effective diameter of the pore, a second layer that still shows important structural and dynamical confinement effects, and the third layer that behaves almost as bulk-like water. Filling of such hydrophilic pores was seen to occur via three main mechanisms: (a) a continuum growth, layer by layer on the pore walls, without nucleation of a liquid plug for pores of ∼1 nm diameter; (b) an axial growth followed by capillary condensation in pores between 2 and 3 nm diameter; and (c) a radial growth with significant supersaturation followed by capillary condensation in the case of larger pores.[14] Although a great deal of effort has been made independently using computational and experimental methodologies, not many examples of a crossed theoretical and experimental approach have been presented so far.[30]

In this work the adsorption of water in nanoporous TiO_2 was studied by NMR and multiscale molecular dynamics simulations. Mesoporous TiO_2 aerosols were synthesized and further characterized by N_2 sorption, rendering a pore diameter of 3.5 nm. Water dynamics in systems with different filling degree were studied by ^1H NMR spectroscopy and double-quantum NMR, where three populations with different mobilities are clearly identified: a highly structured adsorbed layer, a second less structured layer, and a mobile water component which increases with the filling degree. Comparison with multiscale molecular dynamic (MD) simulations enables identification of the capillary condensation onset from which a pore diameter of around 4.5 nm is determined. The difference in the results obtained from N_2 sorption isotherms and from the combination of NMR and MD is ascribed to the presence of a residual first layer of structured water, which is always present due to the high hydrophilicity of the surface. The combination of theoretical and experimental studies is a very powerful tool for complete analysis of the properties of water confined in the mesoporous material, which is critical in applications, such as selective membranes, photocatalysts, and biomaterials.

EXPERIMENTAL SECTION

Synthesis of TiO_2 Porous Materials. Triblock poly(ethylene oxide)-*b*-poly(propylene oxide)-*b*-poly(ethylene oxide) copolymer $EO_{106}PO_{70}EO_{106}$, denoted Pluronic F127 (M_w = 12 600, Aldrich), titanium(IV) isopropoxide 97% (Aldrich), glacial acetic acid (denoted as AcOH, Merck), acetylacetonate (denoted as ACAC, Merck), and ethyl alcohol were used as received. All aqueous solutions were prepared with deionized water having resistivity ≈ 18 M^{-1} cm and degassed using high-purity N_2 (Indura S.A.). The mesoporous TiO_2 aerosols were prepared by evaporation-induced self-assembly using ACAC and AcOH to control Ti(IV) hydrolysis and condensation, as previously performed with Zr(IV) mesoporous thin films.[31] An aqueous precursor mixture (Ti(IV):F127:H_2O:ACAC:AcOH molar composition 1:0.005:2050:9:17) was atomized in a Büchi Spray Dryer model B-290 with a two-fluid nozzle using a secondary airflow of 2.5 N m^3 h^{-1}. The liquid spray was fed into a preheated primary airflow of 44 N m^3 h^{-1}. The temperature of the spray drier inlet gas flow was maintained at 220 °C, and the temperature of the dryer exit was between 115 and 125 °C. The obtained material was calcined at 350 °C using a heating rate of 1 °C min^{-1} for 2 h to remove the template. Details of the aerosol preparation and stability are available elsewhere.[32,33]

Structural Characterization. Scanning electron micrographs (SEM) were obtained using a Supra 40 (Zeiss Company) Field Emission SEM operating at 3 kV, equipped with an Oxford EDS, and transmission electron micrographs were acquired with a Philips EM 301. An ASAP 2420 (Micrometrics) instrument was used to measure the nitrogen adsorption isotherms. Samples were degassed under vacuum at 150 °C overnight prior to measurements at −190 °C. Specific surface area was calculated according to the Brunauer−Emmett−Teller (BET) equation. The total pore volume was calculated by the Gurvich rule at P/P_0 = 0.95, and the apparent micropore volume (for pores smaller than 2 nm in diameter) was determined by *t*-plot using the Harkin−Jura−de Boer equation. The pore size distribution was calculated using the Barrett−Joyner−Halenda (BJH) model.[8]

NMR Experiments. For the NMR studies five samples with different water filling levels were prepared (see Table 1). Equal amounts of the TiO_2 powder sample (0.1000 g) were placed in five separate 4 mm outer diameter zirconia MAS rotors and then dried at 120 °C at reduced pressure (25 in Hg vacuum) for 24 h. One sample (A) was sealed immediately after drying with no extra addition of water. The rest of the samples (B−E)

Table 1. Samples Prepared with Different Filling Degrees of Water: Nomenclature, Relative Humidity, Filling Degree as Determined from NMR and Chemical Shift of the Mobile Component

sample	isopiestic chamber RH	filling degree[b]	signal center [ppm]
A	*a*	0.11	7.85
B	0.43	0.40	6.47
C	0.68	0.48	6.18
D	0.81	0.76	6.14
E	1.00	1.00	5.96

[a]This sample was sealed immediately after the vacuum-drying process. [b]The filling degree was calculated from NMR signal areas corresponding to the two structured layers (s_1, s_2) and the mobile fraction m_f, which for sample E is defined as $s_1 + s_2 + m_f = 1$.

DOI: 10.1021/acs.jpcc.6b12511
J. Phys. Chem. C XXXX, XXX, XXX−XXX

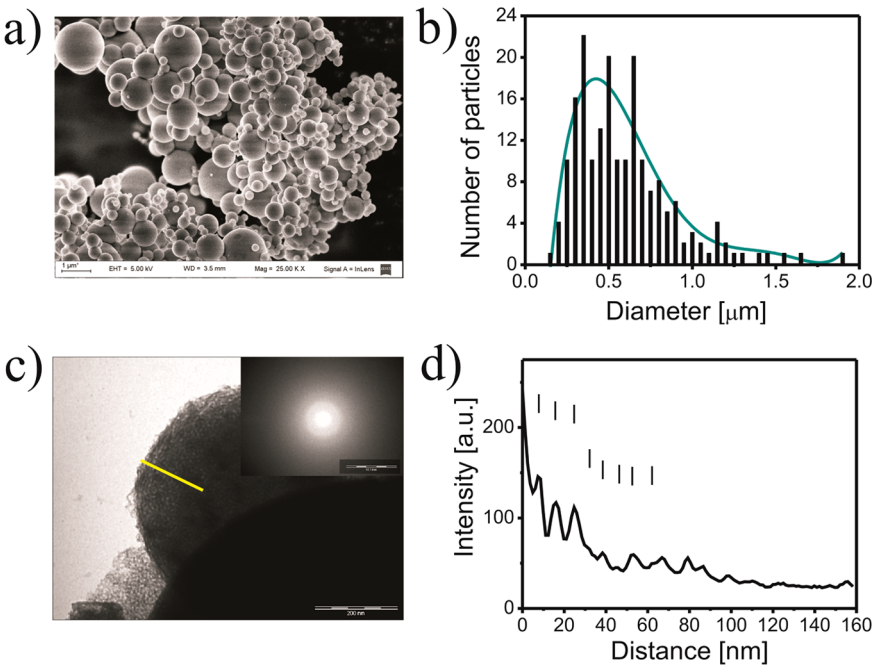

Figure 1. (a) SEM micrograph of the mesoporous TiO_2 aerosol. (b) Size distribution histogram for mesoporous TiO_2. (c) Transmission micrograph of a TiO_2 particle. (d) Profile plot of the zone marked with the yellow line in the TiO_2 transmission micrograph.

were exposed to different relative humidity (RH) in isopiestic chambers for 3 months and then hermetically sealed. The chamber humidity was controlled using pure water and supersaturated solutions of KI, NH_4SO_4, and K_2CO_3.[34] All experiments were performed at 25 °C in a magnetic field of 7 T with a Bruker Avance II-300 spectrometer. Spectra in static conditions were acquired with a DOTY DSI-703 proton-dedicated probe with proton background signal reduction and receiver dead time of 4 μs. High-resolution solid state spectra were recorded using solid state NMR magic angle spinning (SSNMR MAS) with a 4 mm probe. All samples were spun at 10 kHz.

Molecular Dynamics Simulations. All-atom molecular dynamics (MD) simulations of water confined in TiO_2 mesopores of 2.8 and 5.1 nm diameter and 7.1 nm length were performed using the LAMMPS package.[35,36] The VMD program was used for visual analysis of the data.[37] Pores were constructed from bulk crystalline rutile and filled with different numbers of water molecules to obtain pore fillings between 40% and 100%. The density of liquid water inside the pores was determined from canonical simulations in which a condensed phase coexists in equilibrium with a low-density adsorbed phase. Using this value, completely filled pores were constructed. For a comprehensive description of the construction and filling of the pores we refer the interested reader to ref 14. The metal oxide and oxide−water interactions were modeled with the force field developed by Bandura and Kubicki,[38] representing water molecules with the SPC/E potential.[39] Calculations were carried out in the canonical ensemble. All systems were first equilibrated at high temperature and then cooled down to 26.8 °C. Statistical sampling at this final temperature was prolonged for 5 ns, discarding the first nanosecond from further analysis to allow for equilibration. Further details of the simulations' conditions can be found elsewhere.[14]

A separate set of coarse-grained grand canonical molecular dynamics (CG-GCMD) simulations was conducted to estimate the pressure of capillary condensation in pores with dimensions and hydrophilicity similar to the synthesized TiO_2 mesoporous material. In such calculations, water molecules were represented with the mW coarse-grained model.[40] Cylindrical pores with amorphous walls were formed by mW particles, as described in previous reports.[15,41] Water−pore interactions were described in terms of the contact angle, setting a value of 24°, similar to experimental values for mesoporous titania.[42] Capillary condensation pressures were computed in the grand canonical ensemble at 25 °C. Further details on the employed methodology can be found in ref 15.

RESULTS AND DISCUSSION

The size and morphology of the resultant TiO_2 aerosol was determined by SEM and TEM. Scanning electron micrographs confirm the spherical structure of the synthesized aerosols (Figure 1a). An average diameter of ∼500 nm was obtained from analyzing histograms constructed with at least 200 particles from the SEM micrographs (Figure 1b) with 92% submicrometric particles. A typical TEM micrograph corresponding to the TiO_2 aerosol is displayed in Figure 1c with the modulus of the Fourier transform corresponding to the local diffraction pattern. Although the TEM micrograph confirms the presence of porosity, the FFT indicates that this porosity has a local order arrangement. Additionally, Figure 1d shows a profile plot taken on the contour of a particle (line marked in yellow in Figure 1c) where the porosity is more evident.

Figure 2 presents the pore-size distribution curve and the corresponding nitrogen adsorption−desorption isotherms of a TiO_2 sample, where a Type IV curve is obtained. A Type H_2 hysteresis loop is observed, which is characteristic of materials with complex structures and interconnected pore networks. The pore dimensions obtained from the isotherms are 3.5 nm for the diameter and 2.8 nm for the neck, with a surface area of 240 $m^2\ g^{-1}$.[8]

Previous results from molecular dynamics simulations of TiO_2 nanopores show three very different water populations

DOI: 10.1021/acs.jpcc.6b12511
J. Phys. Chem. C XXXX, XXX, XXX−XXX

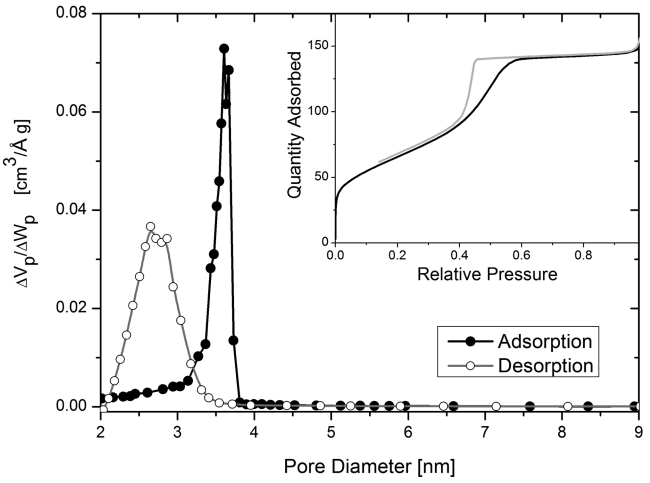

Figure 2. N_2-sorption isotherms (inset) and corresponding pore size distribution curves of the mesoporous TiO_2.

inside the pores: a tightly bound monolayer at the surface, which exhibits solid-like rather than fluid-phase characteristics, a second layer with increased mobility with respect to the first one but still distinctly different from bulk-like water, and finally bulk-like water with uniform density (see Supporting Information).[14] Similar results were observed also for water in the proximity of planar TiO_2.[28,43,44] Figure 3 shows the

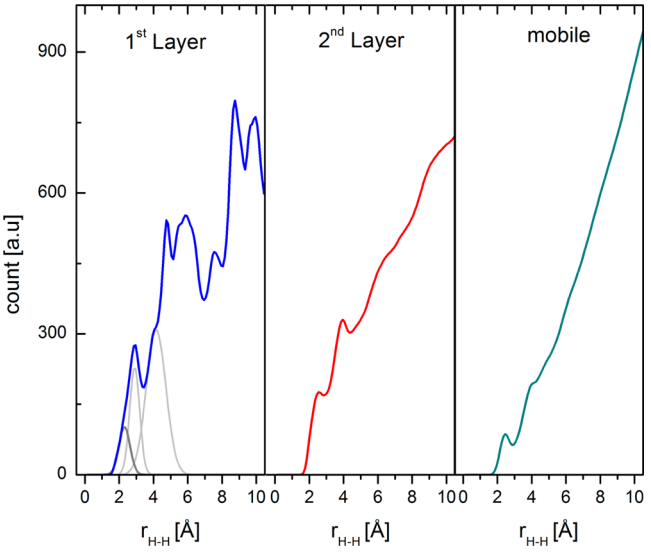

Figure 3. Intermolecular distance distribution between H atoms for molecules in the first, second, and mobile layer (panels left, center, and right, respectively). Results correspond to MD simulations of a 2.8 nm pore completely filled with water.

distances between H−H neighbors within each layer as computed from MD simulations for a 2.8 nm pore completely filled with water. It is observed that the first layer shows more defined distance values due to the strong adsorption of the water molecules to the surface. The molecular mobility increases gradually from the second layer to the bulk, rendering a continuum of distance values. The results from MD for different filling degrees for both 2.8 and 5.1 nm diameters are shown in Figure S1 in the Supporting Information. The distances to the H atoms in the first layer were fitted with Gaussian distributions in order to deconvolute each individual contribution. In Figure 3 only the fitted functions for the smallest distances are shown, and a value of 2.35 Å was obtained for the closest molecules (see Figure S2). Additionally, water layered structure can also be observed in the distances between O−O computed from MD simulations at different water contents inside the pore for both 2.8 and 5.1 nm diameters, which are shown in Figure S3 in the Supporting Information.

For characterization of the water molecules in the first layer, solid state techniques normally applied for the study of solids and polymers were used, resorting to dipolar interactions to determine the structural properties of the material under study. ^{1}H double-quantum experiments (DQ-NMR) were used to measure the larger residual dipolar interactions among the water protons inside the TiO_2 mesopores.[45−49] These measurements allow extraction of very specific localized information. Since the dipolar interaction is inversely related to the cube of the distance between protons, the residual dipolar couplings are a direct measure of the proximity of the involved protons, and so they can bring light to the structural array of the protons of the water molecules inside the mesopores. This experiment can be set with a specific filter which ensures that only those interactions larger than a fixed value are detected.[29] The experiment was set in a way that only the signal arising from those molecules with the largest dipolar interaction were observed, i.e., molecules in the first layer. The result is a very broad spectrum (fwhm 25 kHz) with a doublet structure (see Figure S4 in the Supporting Information). By systematically changing the duration of the interaction with the DQ Hamiltonian, a distribution of dipolar interactions and, consequently, the distance between first neighbors can be obtained (see Supporting Information for further details). In Figure 4 the distribution of the internuclear distances among first neighbors in the first layer obtained from the DQ-NMR is compared to the Gaussian fitting curve of the values obtain from MD calculations. The obtained distance for the closest neighbor of both NMR and simulation is in good agreement, confirming the effectiveness of the DQ-NMR experiment for measurements of confined water. It must be noted that the width of the distributions is different since for the NMR experiment only a small range of dipolar contributions was previously chosen with the filtering process.

Water molecules in the second layer also have a reduced molecular mobility which gives rise to large dipolar interactions. However, a clear separation of signals from the first layer was not possible with DQ-NMR. Therefore, magic angle spinning experiments (MAS) were performed.[50] For ^{1}H MAS NMR, the extent of the residual dipolar line width is inversely proportional to the spinning frequency. Thus, spinning the sample at the magic angle at different frequencies allows a selective improvement in resolution which renders resolved peaks and site-specific information from ^{1}H spectra. This technique has been previously used to study water confined in nanoporous systems of different materials.[11,51,52] A rotation frequency of 10 kHz was used, which means that only those dipolar interactions below 10 kHz can be resolved. It is worth noting that the signal originated by molecules from the first layer does not contribute to the detected signal of this experiment (as it has a larger dipolar interaction) nor the signal arising from mobile molecules with negligible dipolar interactions. A broad spectrum (fwhm ≈ 2.6 kHz) with a doublet is obtained (see Figure S6 in the Supporting Information).

DOI: 10.1021/acs.jpcc.6b12511
J. Phys. Chem. C XXXX, XXX, XXX−XXX

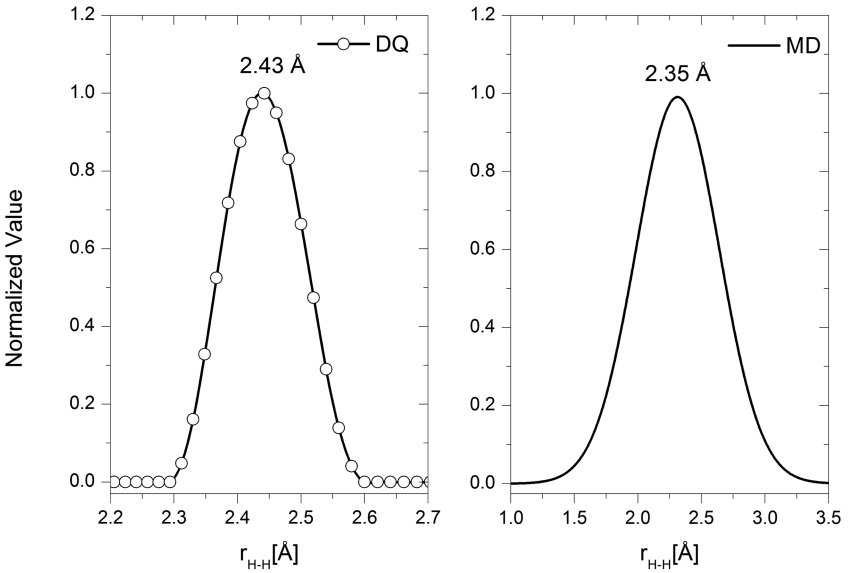

Figure 4. H−H distance obtained from the DQ-NMR experiment and MD calculations for the 2.8 nm pore. This distance corresponds to the spins with the strongest dipolar interaction in the sample, i.e., the closest H pair in the first layer. Solid line in the DQ-NMR was plotted as a guide to the eye.

In the mobile water population, the higher molecular mobility averages significantly the dipolar interactions and the signals are much narrower and intense (fwhm ≈ 600 Hz). Static spectra acquired with a solid-echo[53] pulse sequence were used to detect the signal corresponding to all of the water contained in the porous systems. Deconvolution of these signals was carried out using the information obtained via the DQ and MAS spectra as shown in Figure 5. Figure 5a shows data corresponding to sample A, with a low level of water filling, for which the contribution of the DQ and MAS spectra accounts for the deconvolution of the whole spectrum, that is, mobile water is not present in this sample. On the other hand, for sample C (filling degree = 0.48) an intense narrow line at the center of the spectrum, characteristic of a mobile fraction, is observed (Figure 5b). In both cases a very broad signal with low intensity is present, which can be assigned to the OH groups of the TiO_2 surface.

The filling degree was calculated from the NMR experiments using the deconvoluted areas of the first two layers (s_1, s_2) and the mobile fraction m_f, where for sample E the filling is defined as $s_1 + s_2 + m_f = 1$. Sample E was used as a normalization value for the rest of the systems, considering that in this case the nanopores are completely filled with water. The results for each sample are shown in Figure 6a. In all cases, the amount of water in the first two layers (signals obtained through DQ and MAS experiments, respectively) remains constant within the experimental error, indicating that structured water is present even at very low filling degrees. Moreover, with the applied protocol, even sample A retains practically the same amount of structured water (ca. 10%) as the rest of the systems. Although more severe drying procedures were tried, due to the highly hygroscopic character of the material, water could not be completely removed and the filling degree is not zero. This result is in agreement with previous reports which show that temperatures around 530 °C are needed to fully remove water from the TiO_2 surface.[54−56] The fact that all systems present the same amount of water in the first layer is consistent with the distance for the closest neighbors obtained through the DQ experiment, which is the same in every sample (see Figure S5).

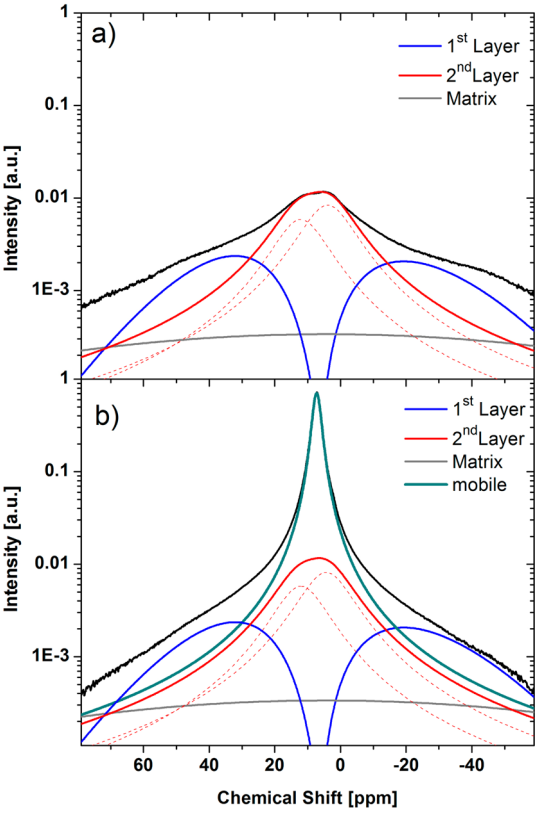

Figure 5. Spectra acquired in static conditions with a solid-echo pulse sequence. (a) In sample A two structured layers of water molecules are identified, where the dotted lines show the deconvolution of the second water layer. (b) Sample C (filling degree = 0.56). An extra contribution originated in more mobile water is observed. Logarithmic scale is used to evidence the broad contribution from the matrix and the more structured water layers.

These results are in agreement with the MD simulations for all filling degrees as shown in the Supporting Information.

DOI: 10.1021/acs.jpcc.6b12511
J. Phys. Chem. C XXXX, XXX, XXX−XXX

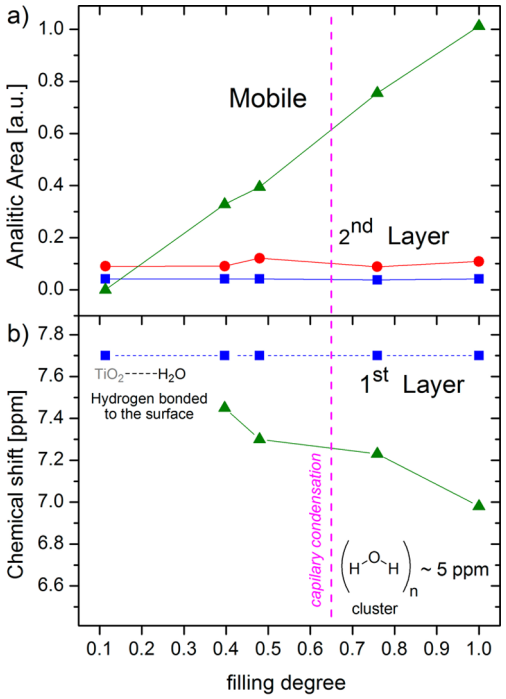

Figure 6. (a) Composition of the mobile fraction and the two structured water layers as a function of the filling degree obtained from NMR experiments. (b) Chemical shift position of the mobile and first layer of water. As the filling degree increases mobile water signals shift toward lower values, approaching the bulk water behavior. For the description of capillary condensation see Figure 7.

On the other hand, the proportion of mobile and structured water is not the same for the different samples but strongly depends on the water pore filling at every RH value (Figures 6, S1, and S3). As the amount of water in the mobile fraction increases, its molecular mobility increases accordingly; thus, it is expected that its signal is shifted to lower ppm values as the filling degree increases (see Figure 6b). In order to explain this phenomenon, it is necessary to recall that water molecules of the mobile fraction are subject to several environments, and the resulting chemical shift is the weighted average of all of the present species. A similar behavior was observed and analyzed in silica nanopores.[11] It is expected that water molecules diffusing in very mobile clusters behave more like bulk water, with its chemical shift being close to the bulk water value (4.7–5 ppm). On the contrary, the chemical shift position of the more structured layer remains unchanged since water molecules are interacting through hydrogen bonds with the surface. It has been reported that water in strong interaction with different TiO_2 materials exhibits higher chemical shift values.[28,29,56]

To rationalize the experimental behavior observed by NMR we studied the structure and composition of water confined in titania nanopores with different water content resorting to all-atom molecular dynamics simulations. The dimensions of the simulated pores (2.8 and 5.1 nm diameter) are in the range of the synthesized mesoporous materials. Previous molecular dynamics simulations[14] suggested that the water filling mechanism depends strongly on the pore radius. For very small pores (1.3 nm diameter) a continuum growth without nucleation of a liquid plug was observed. In larger pores, the filling starts homogeneously forming a strongly adsorbed bilayer, but a further increase in the number of water molecules in the pores ultimately leads to capillary condensation. The diameter of the pore determines the extent of supersaturation required for condensation.

In what follows we analyze the composition of the water populations inside the pores. In Figure 7a and 7c, the fraction of molecules in each layer is plotted as a function of the filling degree for two different nanopore sizes. The definition of the first, second, and mobile layers is based on the radial density profiles (local densities of water along the radial direction of the pore) of completely filled pores, as shown in Figure S7 (Supporting Information). In Figure 7a and 7b the vertical dashed line indicates the filling at which capillary condensation takes place, according to previous canonical ensemble simulations.[14] The first and second layers form at a very low filling degree for both pores, in accordance with the experimental results shown in Figure 6. The difference between the two pores is how this capillary condensation onset is reached. For 2.8 nm pore diameter, the vapor–liquid transition occurs in equilibrium with little or none supersaturation. This can be observed in the sudden increase in the mobile water fraction in the pore (green curve Figure 7a) and also in the radial density profiles for different filling fractions in Figure 7c. It can be seen that increasing water content leads to formation of the first and second layers, and then capilary condensation occurs without the appearance of water aggregates toward the center of the pore. The gray shaded area corresponds to the difference in the water density before and after the appearance of a liquid plug occurs, and it can be seen that in the case of the 2.8 nm pore it is very small. However, for 5.1 nm pores radial growth occurs, with the appearance of water aggregates (Figure 7d) with structural and dynamical characteristics of bulk-like water, as characterized in a previous report.[14] This translates in an almost linear increase of the mobile fraction with the filling factor, as can be seen in Figure 7b. On the basis of the molecular detail provided from the MD results, the experimental behavior observed by NMR and shown in Figure 6 is compatible with large hydrophilic pores in which capillary condensation occurs preceded by an important supersaturation.

The structural characterization of water inside titania nanopores from both NMR experiments and MD simulations can help to rationalize the experimental adsorption isotherm presented in Table 1 (filling degree vs RH). From the NMR experiments it is possible to see that capillary condensation occurs for a RH of 0.81 approximately with a filling of the pore of 80%. Both the capillary condensation pressure and the filling degree are rather high for pores of sizes in the range of 3 nm, as obtained from characterization of the TiO_2 aerosols (Figure 2). Besides, pores of 2.8/3.5 nm size are rather small for TiO_2 templated with Pluronics F127, since this synthetic system usually renders thin films and aerogels with pores ranging from 5 to11 nm size.[42,57,58] The observation of such a high filling of the pore before capillary condensation is a clear sign of an important supersaturation, as discussed in the previous paragraph based on MD and NMR results. The value of water capillary pressure is similar to reported results for larger titania mesopores.[42,59] This discrepancy could be explained by the presence of the compact water bilayer in the pores as observed by NMR and MD experiments. Indeed, this bilayer is strongly adsorbed and could not be eliminated even after severe drying procedures (sample A) due to the high hydrophilicity of the material. As a consequence, the effective or accessible diameter of the TiO_2 nanopores is around 1 nm smaller than the physical diameter. This means that the pore/necks measured by nitrogen adsorption–desorption isotherms

DOI: 10.1021/acs.jpcc.6b12511
J. Phys. Chem. C XXXX, XXX, XXX–XXX

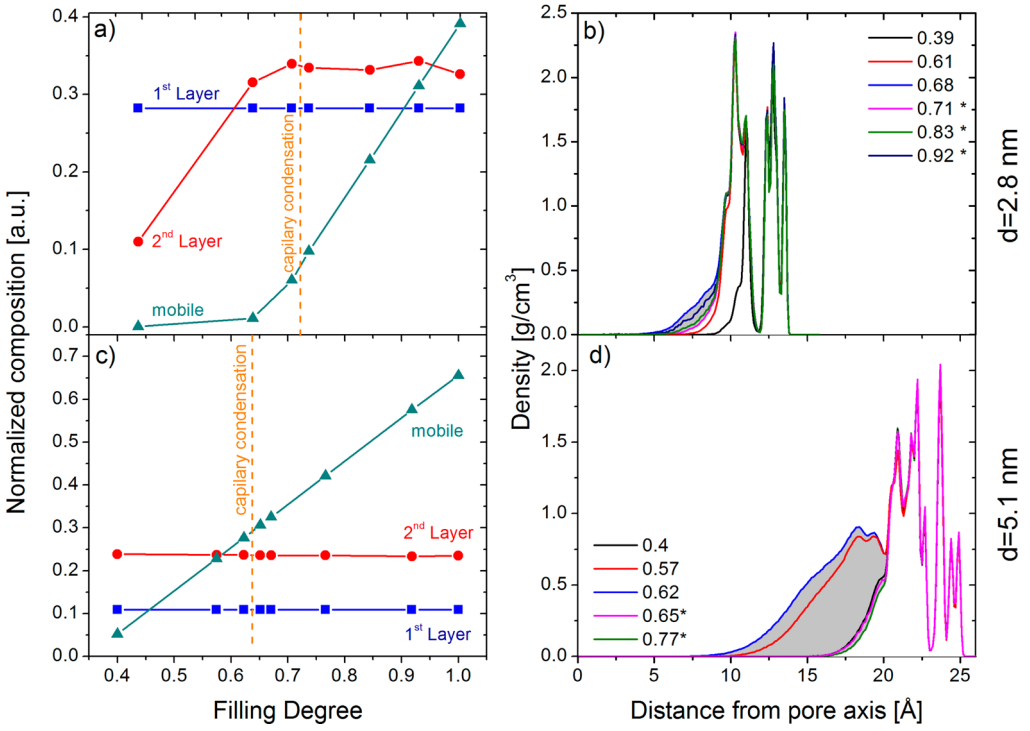

Figure 7. Composition of the mobile fraction and the two structured water layers from MD simulations of nanopores of 2.8 and 5.1 nm diameter (a and c, respectively) with different filling degrees. (b and d) Radial density profiles as a function of the density from the pore axis (considering the position of the oxygen atoms of the water molecules) for nanopore diameters of 2.8 and 5.1 nm, respectively. Filling degree of each curve is indicated in the legend, and the asterisk refers to filling for which capillary condensation is observed. In those cases, the radial density plotted corresponds to the adsorbed phase in equilibrium with the liquid phase (whose density is not shown). Gray shaded areas indicate the difference between the profiles just before and after capillary condensation, highlighting that the vapor−liquid transition occurs in equilibrium (no supersaturation) for the 2.8 nm nanopore, whereas a significant supersaturation is observed for the 5.1 nm pore.

(Figure 2) correspond to the nanopores plus the adsorbed bilayer, with the reported values of 2.8 and 3.5 nm representing the accessible diameters and the physical diameters being around 3.8/4.5 nm. This range of sizes is compatible with the observed supersaturation prior to capillary condensation. Finally, the capillary condensation pressure observed experimentally around 0.8 is in accordance with grand canonical MD simulations conducted in this work for cylindrical pores of 4 nm diameter and a water contact angle of 25° that rendered a value of 0.825, similar to reported results for mesoporous titania.[42]

CONCLUSIONS

In this work, we synthesized mesoporous TiO_2 aerosols which were characterized by SEM and TEM. A spherical particle morphology was found with an average diameter of 500 nm. Nitrogen adsorption−desorption isotherms present a type IV curve with a hysteresis loop, characteristic of materials with interconnected pore networks. The diameter obtained was 3.5 and 2.8 nm for the neck. The water filling mechanism in the nanopores was studied by NMR and contrasted with MD simulations for different filling factors. ^{1}H static spectroscopy, MAS SSNMR, and DQ-NMR experiments show the existence of three different layers of water as previously predicted by MD simulations. The first layer of strongly adsorbed water molecules was found for all filling degrees, due the high hydrophilicity of the TiO_2 surface and characterized by DQ-NMR. The second, more mobile layer was characterized through MAS spectra, while the inner liquid layer was clearly detected by static spectra. The NMR data can be used to build a filling curve, where supersaturation prior to capillary condensation is observed in agreement with the behavior qualitatively described by MD simulations for pore diameters of 3.8 nm. It was found that N_2 adsorption isotherms give an accessible diameter lower than that observed by molecular dynamics and NMR due to the approximately 1 nm layer of structured water. Such a detailed analysis of the water dynamics presented in this work was only possible due to the synergistic combination of experimental NMR data and MD simulations.

ASSOCIATED CONTENT

Supporting Information

The Supporting Information is available free of charge on the ACS Publications website at DOI: 10.1021/acs.jpcc.6b12511.

Detailed explanation of the DQ NMR pulse sequence and experiment; distances between intermolecular O or H and the radial density of water obtained by MD simulations of a 2.8 and 5.1 nm pore with different filling degree (PDF)

AUTHOR INFORMATION

Corresponding Authors

*E-mail: racosta@famaf.unc.edu.ar.

*E-mail: gsoler-illia@unsam.edu.ar.

ORCID

Manuel I. Velasco: 0000-0003-1500-4672

Damián Scherlis: 0000-0002-0588-287X

Galo J. A. A. Soler-Illia: 0000-0001-9984-3806

Notes

The authors declare no competing financial interest.

DOI: 10.1021/acs.jpcc.6b12511
J. Phys. Chem. C XXXX, XXX, XXX−XXX

■ ACKNOWLEDGMENTS

We are thankful for financial support from Agencia Nacional de Promoción Científica y Tecnológica (PICT 2015-3526), SECyT-UNC, and CONICET. E.A.F. and G.J.A.A.S.I are permanent research fellows of CONICET. We also thank Dr. Andrés Zelcer and Dra. Verónica Lombardo for their assistance in the synthesis and characterization of the TiO_2 aerosols.

■ REFERENCES

(1) Davis, M. E. Ordered Porous Materials for Emerging Applications. *Nature* **2002**, *417*, 813−821.
(2) Li, W.; Zhao, D. An Overview of the Synthesis of Ordered Mesoporous Materials. *Chem. Commun.* **2013**, *49*, 943−946.
(3) Corma, A. From Microporous to Mesoporous Molecular Sieve Materials and Their Use in Catalysis. *Chem. Rev.* **1997**, *97*, 2373−2419.
(4) Li, W.; Wu, Z.; Wang, J.; Elzatahry, A. A.; Zhao, D. A Perspective on Mesoporous TiO2Materials. *Chem. Mater.* **2014**, *26*, 287−298.
(5) Bhanja, P.; Bhaumik, A. Porous Nanomaterials as Green Catalyst for the Conversion of Biomass to Bioenergy. *Fuel* **2016**, *185*, 432−441.
(6) Azaïs, T.; Tourné-Péteilh, C.; Aussenac, F.; Baccile, N.; Coelho, C.; Devoisselle, J. M.; Babonneau, F. Solid-State NMR Study of Ibuprofen Confined in MCM-41 Material. *Chem. Mater.* **2006**, *18*, 6382−6390.
(7) Viva, F. A.; Bruno, M. M.; Franceschini, E. A.; Thomas, Y. R. J.; Ramos Sanchez, G.; Solorza-Feria, O.; Corti, H. R. Mesoporous Carbon as Pt Support for PEM Fuel Cell. *Int. J. Hydrogen Energy* **2014**, *39*, 8821−8826.
(8) Rouquerol, J.; Rouquerol, F.; Llewellyn, P.; Maurin, G.; Sing, K. S. *Adsorption by Powders and Porous Solids: Principles, Methodology and Applications.*; Elsevier: New York, 2013
(9) Li, Q.; Song, J.; Besenbacher, F.; Dong, M. Two-Dimensional Material Confined Water. *Acc. Chem. Res.* **2015**, *48*, 119−127.
(10) Steiner, E.; Bouguet-Bonnet, S.; Blin, J.-L.; Canet, D. Water Behavior in Mesoporous Materials as Studied by NMR Relaxometry. *J. Phys. Chem. A* **2011**, *115*, 9941−9946.
(11) Grünberg, B.; Emmler, T.; Gedat, E.; Shenderovich, I.; Findenegg, G. H.; Limbach, H. H.; Buntkowsky, G. Hydrogen Bonding of Water Confined in Mesoporous Silica MCM-41 and SBA-15 Studied by 1H Solid-State NMR. *Chem. - Eur. J.* **2004**, *10*, 5689−5696.
(12) Shirono, K.; Daiguji, H. Molecular Simulation of the Phase Behavior of Water Confined in Silica Nanopores. *J. Phys. Chem. C* **2007**, *111*, 7938−7946.
(13) Yamashita, K.; Daiguji, H. Molecular Dynamics Simulations of Water Uptake into a Silica Nanopore. *J. Phys. Chem. C* **2015**, *119*, 3012−3023.
(14) Solveyra, E. G.; del la Llave, E.; Molinero, V.; Soler-Illia, G. J. A. A.; Scherlis, D. A. Structure, Dynamics, and Phase Behavior of Water in TiO2 Nanopores. *J. Phys. Chem. C* **2013**, *117*, 3330−3342.
(15) Factorovich, M. H.; Gonzalez Solveyra, E.; Molinero, V.; Scherlis, D. A. Sorption Isotherms of Water in Nanopores: Relationship Between Hydropohobicity, Adsorption Pressure, and Hysteresis. *J. Phys. Chem. C* **2014**, *118*, 16290−16300.
(16) Bonnaud, P. A.; Coasne, B.; Pellenq, R. J.-M. Molecular Simulation of Water Confined in Nanoporous Silica. *J. Phys.: Condens. Matter* **2010**, *22*, 284110.
(17) Milischuk, A. A.; Ladanyi, B. M. Structure and Dynamics of Water Confined in Silica Nanopores. *J. Chem. Phys.* **2011**, *135*, 174709.
(18) Bourg, I. C.; Steefel, C. I. Molecular Dynamics Simulations of Water Structure and Diffusion in Silica Nanopores. *J. Phys. Chem. C* **2012**, *116*, 11556−11564.
(19) Yamashita, K.; Daiguji, H. Molecular Simulations of Water Adsorbed on Mesoporous Silica Thin Films. *J. Phys. Chem. C* **2013**, *117*, 2084−2095.
(20) Renou, R.; Szymczyk, A.; Ghoufi, A. Influence of the Pore Length on the Properties of Water Confined in a Silica Nanopore. *Mol. Phys.* **2014**, *112*, 2275−2281.
(21) Milischuk, A. A.; Krewald, V.; Ladanyi, B. M. Water Dynamics in Silica Nanopores: The Self-Intermediate Scattering Functions. *J. Chem. Phys.* **2012**, *136*, 224704.
(22) Chen, X.; Mao, S. S. Titanium Dioxide Nanomaterials: Synthesis, Properties, Modifications and Applications. *Chem. Rev.* **2007**, *107*, 2891−2959.
(23) Gerasimova, T. V.; Evdokimova (Galkina), O. L.; Kraev, A. S.; Ivanov, V. K.; Agafonov, A. V. Micro-Mesoporous Anatase TiO2 Nanorods with High Specific Surface Area Possessing Enhanced Adsorption Ability and Photocatalytic Activity. *Microporous Mesoporous Mater.* **2016**, *235*, 185−194.
(24) Coakley, K. M.; McGehee, M. D. Photovoltaic Cells Made from Conjugated Polymers Infiltrated into Mesoporous Titania. *Appl. Phys. Lett.* **2003**, *83*, 3380−3382.
(25) Mor, G. K.; Varghese, O. K.; Paulose, M.; Shankar, K.; Grimes, C. A. A Review on Highly Ordered, Vertically Oriented TiO2 Nanotube Arrays: Fabrication, Material Properties, and Solar Energy Applications. *Sol. Energy Mater. Sol. Cells* **2006**, *90*, 2011−2075.
(26) Fujishima, A.; Zhang, X.; Tryk, D. A. TiO2 Photocatalysis and Related Surface Phenomena. *Surf. Sci. Rep.* **2008**, *63*, 515−582.
(27) Nosaka, A. Y.; Kojima, E.; Fujiwara, T.; Yagi, H.; Akutsu, H.; Nosaka, Y. Photoinduced Changes of Adsorbed Water on a TiO_2 Photocatalytic Film As Studied by ^1H NMR Spectroscopy. *J. Phys. Chem. B* **2003**, *107*, 12042−12044.
(28) Nosaka, A. Y.; Fujiwara, T.; Yagi, H.; Akutsu, H.; Nosaka, Y. Characteristics of Water Adsorbed on TiO_2 Photocatalytic Systems with Increasing Temperature as Studied by Solid-state ^1H NMR Spectroscopy. *J. Phys. Chem. B* **2004**, *108*, 9121−9125.
(29) Zhu, L.; Gu, Q.; Sun, P.; Chen, W.; Wang, X.; Xue, G. Characterization of the Mobility and Reactivity of Water Molecules on TiO_2 Nanoparticles by ^1H Solid-State Nuclear Magnetic Resonance. *ACS Appl. Mater. Interfaces* **2013**, *5*, 10352−10356.
(30) Pajzderska, A.; Gonzalez, M. A.; Mielcarek, J.; Wąsicki, J. Water Behavior in MCM-41 as a Function of Pore Filling and Temperature Studied by NMR and Molecular Dynamics Simulations. *J. Phys. Chem. C* **2014**, *118*, 23701−23710.
(31) Zelcer, A.; Soler-Illia, G. J. A. A. One-Step Preparation of UV Transparent Highly Ordered Mesoporous Zirconia Thin Films. *J. Mater. Chem. C* **2013**, *1*, 1359.
(32) Zelcer, A.; Franceschini, E.; Lombardo, M. V.; Soler-IIlia, G. S. A. A. General Method to Produce Mesoporous Transition Metal Oxide Spherical Particles from Aqueous-Based Media Spray Drying. Submitted for publication.
(33) Soler Illia, G. J. A. A.; Zelcer, A.; Lombardo, M. V.; Franceschini, E. Un Procedimiento Para La Obtención de Partículas Esféricas de Óxidos Metálicos Mesoporosos de Composición, Área Superficial, Porosidad Y Tamaño Controlados. Argentine Patent 20150104299, December 28, 2015.
(34) Greenspan, L. Humidity Fixed Points of Binary Saturated Aqueous Solutions. *J. Res. Natl. Bur. Stand., Sect. A* **1977**, *81A*, 89.
(35) Plimpton, S. Fast Parallel Algorithms for Short-Range Molecular Dynamics. *J. Comput. Phys.* **1995**, *117*, 1−19.
(36) *LAMMPS, Molecular Dynamics Simulator*; Sandia, http://lammps.sandia.gov.
(37) Humphrey, W.; Dalke, A.; Schulten, K. VMD: Visual Molecular Dynamics. *J. Mol. Graphics* **1996**, *14*, 33−38.
(38) Bandura, A. V.; Kubicki, J. D. Derivation of Force Field Parameters for TiO_2-H_2O Systems from a Initio Calculations. *J. Phys. Chem. B* **2003**, *107*, 11072−11081.
(39) Berendsen, H. J. C.; Grigera, J. R.; Straatsma, T. P. The Missing Term in Effective Pair Potentials. *J. Phys. Chem.* **1987**, *91*, 6269−6271.
(40) Molinero, V.; Moore, E. B. Water Modeled as an Intermediate Element between Carbon and Silicon. *J. Phys. Chem. B* **2009**, *113*, 4008−4016.
(41) González Solveyra, E.; de la Llave, E.; Scherlis, D. A.; Molinero, V. Melting and Crystallization of Ice in Partially Filled Nanopores. *J. Phys. Chem. B* **2011**, *115*, 14196−14204.
(42) Violi, I. L.; Perez, M. D.; Fuertes, M. C.; Soler-Illia, G. J. A. A. Highly Ordered, Accessible and Nanocrystalline Mesoporous TiO_2

DOI: 10.1021/acs.jpcc.6b12511
J. Phys. Chem. C XXXX, XXX, XXX−XXX

Thin Films on Transparent Conductive Substrates. *ACS Appl. Mater. Interfaces* **2012**, *4*, 4320−4330.
(43) Wei, M. J.; Zhou, J.; Lu, X.; Zhu, Y.; Liu, W.; Lu, L.; Zhang, L. Diffusion of Water Molecules Confined in Slits of Rutile TiO_2(110) and graphite(0001). *Fluid Phase Equilib.* **2011**, *302*, 316−320.
(44) Předota, M.; Bandura, A. V.; Cummings, P. T.; Kubicki, J. D.; Wesolowski, D. J.; Chialvo, A. A.; Machesky, M. L. Electric Double Layer at the Rutile (110) Surface. 1. Structure of Surfaces and Interfacial Water from Molecular Dynamics by Use of Ab Initio Potentials. *J. Phys. Chem. B* **2004**, *108*, 12049−12060.
(45) Graf, R.; Heuer, A.; Spiess, H. W. Chain-Order Effects in Polymer Melts Probed by 1H Double-Quantum NMR Spectroscopy. *Phys. Rev. Lett.* **1998**, *80*, 5738−5741.
(46) Voda, M. A.; Demco, D. E.; Perlo, J.; Orza, R. A.; Blümich, B. Multispin Moments Edited by Multiple-Quantum NMR: Application to Elastomers. *J. Magn. Reson.* **2005**, *172*, 98−109.
(47) Saalwächter, K. Proton Multiple-Quantum NMR for the Study of Chain Dynamics and Structural Constraints in Polymeric Soft Materials. *Prog. Nucl. Magn. Reson. Spectrosc.* **2007**, *51*, 1−35.
(48) Acosta, R. H.; Vega, D. A.; Villar, M. A.; Monti, G. A.; Vallés, E. M. Double Quantum NMR Applied to Polymer Networks with Low Concentration of Pendant Chains. *Macromolecules* **2006**, *39*, 4788−4792.
(49) Acosta, R. H.; Monti, G. A.; Villar, M. A.; Vallés, E. M.; Vega, D. A. Transiently Trapped Entanglements in Model Polymer Networks. *Macromolecules* **2009**, *42*, 4674−4680.
(50) Brown, S. P. Applications of High-Resolution ^{1}H Solid-State NMR. *Solid State Nucl. Magn. Reson.* **2012**, *41*, 1−27.
(51) Suzuki, Y.; Steinhart, M.; Graf, R.; Butt, H. J.; Floudas, G. Dynamics of Ice/Water Confined in Nanoporous Alumina. *J. Phys. Chem. B* **2015**, *119*, 14814−14820.
(52) Xu, Y.; Watermann, T.; Limbach, H.-H.; Gutmann, T.; Sebastiani, D.; Buntkowsky, G. Water and Small Organic Molecules as Probes for Geometric Confinement in Well-Ordered Mesoporous Carbon Materials. *Phys. Chem. Chem. Phys.* **2014**, *16*, 9327−9336.
(53) Boden, N.; Mortimer, M. An NMR "solid" echo Experiment for the Direct Measurement of the Dipolar Interactions between Spin- 1 2 Pairs in Solids. *Chem. Phys. Lett.* **1973**, *21*, 538−540.
(54) Yamamoto, S.; Bluhm, H.; Andersson, K.; Ketteler, G.; Ogasawara, H.; Salmeron, M.; Nilsson, A. In Situ X-Ray Photoelectron Spectroscopy Studies of Water on Metals and Oxides at Ambient Conditions. *J. Phys.: Condens. Matter* **2008**, *20*, 184025.
(55) LunPang, C.; Lindsay, R.; Thornton, G. Chemical Reactions on Rutile TiO_2(110). *Chem. Soc. Rev.* **2008**, *37*, 2328−2353.
(56) Bavykin, D. V.; Carravetta, M.; Kulak, A. N.; Walsh, F. C. Application of Magic-Angle Spinning NMR to Examine the Nature of Protons in Titanate Nanotubes. *Chem. Mater.* **2010**, *22*, 2458−2465.
(57) Martínez, E. D.; Boissière, C.; Grosso, D.; Sanchez, C.; Troiani, H.; Soler-Illia, G. J. A. A. Confinement-Induced Growth of Au Nanoparticles Entrapped in Mesoporous TiO_2 Thin Films Evidenced by in Situ Thermo-Ellipsometry. *J. Phys. Chem. C* **2014**, *118*, 13137−13151.
(58) Frančič, N.; Bellino, M. G.; Soler-Illia, G. J. A. A.; Lobnik, A. Mesoporous Titania Thin Films as Efficient Enzyme Carriers for Paraoxon Determination/detoxification: Effects of Enzyme Binding and Pore Hierarchy on the Biocatalyst Activity and Reusability. *Analyst* **2014**, *139*, 3127−3136.
(59) Fuertes, M. C.; Colodrero, S.; Lozano, G.; González-Elipe, A. R.; Grosso, D.; Boissière, C.; Sanchez, C.; Soler-Illia, G. J. D. A. A.; Míguez, H. Sorption Properties of Mesoporous Multilayer Thin Films. *J. Phys. Chem. C* **2008**, *112*, 3157−3163.

DOI: 10.1021/acs.jpcc.6b12511
J. Phys. Chem. C XXXX, XXX, XXX−XXX